LANGMUIR

pubs.acs.org/Langmuir Article

Surface Tension Measurements of Aqueous Liquid−Air Interfaces Probed with Microscopic Indentation

Chathuri P. Kaluarachchi, Hansol D. Lee, Yiling Lan, Thiranjeewa I. Lansakara, and Alexei V. Tivanski*

Cite This: *Langmuir* 2021, 37, 2457−2465 Read Online

ACCESS | Metrics & More | Article Recommendations

ABSTRACT: To elucidate the intricate role that the sea surface microlayer (SML) and sea spray aerosols (SSAs) play in climate, understanding the chemical complexity of the SML and how it affects the physical−chemical properties of the microlayer and SSA are important to investigate. While the surface tension of the SML has been studied previously using conventional experimental tools, accurate measurements must be localized to the thickness of the air−liquid interface of the SML. Here we explore the atomic force microscopy (AFM) capabilities to quantify the surface tension of aqueous solution droplets with (sub)micrometer indentation depths into the interface. Sample droplets of hexanoic acid at molar concentrations ranging from 0.1 to 80 mM and SML from a recent wave flume study were investigated. A constant-radius AFM nanoneedle was used to probe ca. 200 μL droplets with 0.3−1.2 μm indentation depths. As a comparison, the surface tension of bulk samples was also measured using a conventional force tensiometer. The data for the hexanoic acid show an excellent overlap between the AFM and force tensiometer surface tension measurements. For the surface tension measurements of the SML, however, the measured values from the AFM were 2.5 mN/m lower than that from the force tensiometer, which was attributed to the structural and chemical complexity of the SML, differences in the probing depth for each method, and the time scale required for the surface film to restructure as the needle is retracted away from the liquid surface. Overall, the study confirmed the accuracy of the AFM method in quantifying the surface tension of aqueous solutions over a wide range of concentrations for surface-active organic compounds. The methodology can be further used to reveal small, yet important, differences in the surface tension of complex air−liquid interfaces such as liquid systems where the type and concentration of surfactants vary with the distance from the air−liquid interface. For such complex systems, AFM measurements of the surface tension as a function of the probing depth and pulling rate may reveal a sublayer film structure of the liquid interface.

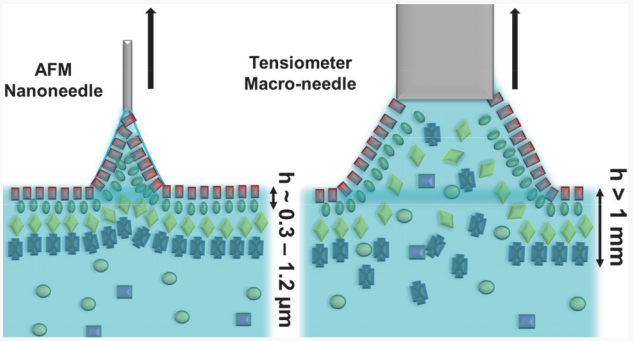

INTRODUCTION

Seawater is a complex mixture of organic, inorganic, and biological compounds.[1] The topmost layer of the seawater, which is highly enriched in a variety of organic species, is called the sea surface microlayer (SML).[2−5] The SML is a highly complex thin film that contains multilayers of surface-active and surface-inactive chemical and biological species such as fatty acids, proteins, lipids, and polysaccharides primarily of natural origin.[2,4,6−11] Seawater and the SML play important roles in regulating the climate because they are the sources of primary sea spray aerosols (SSAs).[12,13] With the wave breaking of seawater, the formed bubbles rise to the top while scavenging organic species and enriching the SML.[12,14,15] Upon bursting, the bubbles release SSAs through film and jet droplet formation mechanisms.[6] In this way, the chemical composition of the SML modulates the composition and physical−chemical properties of the SSAs.[16] Because of the complex chemical nature of the SML and its role in the selective enrichment of various chemical species into the aerosol, SSAs are highly complex mixtures of many chemical and biological compounds at various mixing states and morphologies.[12] This in turn strongly affects the chemical and physical properties of SSAs in the atmosphere.[2,14,17−20] Once airborne, an SSA can directly scatter solar radiation (direct effect) or act as cloud condensation nuclei that facilitate the formation of cloud droplets (indirect effect), with the overall aerosol effect leading to global cooling.[13,17,18,20]

While many have studied the SML, uncertainties still exist regarding their exact thickness and interfacial structure. One study showed that the SML is composed of marine nanolayers

Received: December 10, 2020
Revised: January 30, 2021
Published: February 12, 2021

https://dx.doi.org/10.1021/acs.langmuir.0c03507
Langmuir 2021, 37, 2457−2465

with thicknesses of between 1 and 10 nm.[21] Additionally, the bubble film at bursting which governs the generation of SSA film drops has a reported thickness of between 10−1000 nm, with the film structure likely resembling the topmost surfactant film layers of the SML.[22,23] A different study defined the SML as a gel-like layer with components such as dissolved polymeric carbohydrates, amino acids, and gel particles, with reported thicknesses of between 20 and 150 μm.[6,24] A third study reported the apparent sampling thickness of the SML of 50 ± 10 μm.[25,26] Despite the inconsistency, however, it is well established that both water-soluble and insoluble surfactants partition to the air−water interface of the SML, which can alter the hydrodynamic properties of the interface by forming a physical−chemical barrier.[2,10,27] In this regard, the degree of the organic enrichment and surfactant packing to form surface films could be understood by measuring the surface tension. Laboratory and field measurements show that the SML surface tension can be significantly reduced with the formation of the surface films.[8,10,28,29] The surface tension of the SML was also shown to be sensitive to changes in the production flux, size, and residence time of air bubbles.[8,30,31] Hence, it will be especially imperative to develop experimental approaches that enable measurements of the surface tension of SML and SML-related model systems at the topmost interfacial layer where a relatively high concentration of surface-active compounds and the presence of surface films are expected.[10,25,32]

There are several experimental methods available that can measure the surface tension of liquid systems of varying thicknesses and volumes.[33−39] For example, the surface tension of microsized droplets (1−4 pL) can be quantified with optical tweezers, which trap a suspended droplet and measure the backscattered Raman signal to quantify the droplet surface tension.[38] Another method is the microfluidic device which uses high-speed imaging of immiscible droplets (40−150 μm) to collect optical images, and the data are related to the droplet interfacial tension using the Taylor plots.[39] Additionally, the surface tension can be quantified using the pendant drop method which captures images of the hanging droplet's curvature (5−20 μL) to determine the balance of forces between the capillary tube and the droplet and quantify the surface tension.[33,40,41] Finally, the force tensiometer which includes a Du Noüy tensiometer and Wilhelmy plate techniques is a conventional macroscopic method commonly used to measure the surface tension of bulk liquids (ca. 10 mL and approximately 1−10 mm in probing depth into the air−liquid interface).[33,35,36,42−44] In these force tensiometer methods, a platinum ring, a metal plate, or a cylindrical wire is used to probe the liquid−air interface and measure the retraction force required to break away from the interface, which is used to quantify the surface tension. Nevertheless, none of these experimental techniques allow for the localized measurement of surface tension on the tens to hundreds of nanometers thick interfaces. Therefore, this constraint limits the applicability of these techniques to accurate measurements of the SML's surface tension at the topmost interfacial layer where thin surfactant multilayers are expected. Recently, however, an atomic force microscope (AFM) was used to directly quantify the surface tension of liquid droplets. A custom-made AFM constant-diameter nanoneedle probe was able to indent the liquid droplet with controlled indentation depths of tens to hundreds of nanometers. The maximum retention force as the probe moved away from the liquid interface was measured to quantify the surface tension of the liquid.[45−49] This was shown to be widely applicable to different liquid samples, from substrate-deposited individual submicrometer droplets and SSA[45,47,49,50] to ionic liquids.[46,51,52]

Herein, the AFM-based surface tension methodology is further developed to study the aqueous liquid−air interfaces of macroscopic droplets with volumes on the order of 200 μL. The study was conducted under ambient temperature and pressure by probing the liquid droplet systems with controlled indentation depths ranging from 0.3 to 1.2 μm to measure the maximum retention force. To minimize the liquid evaporation, the study was conducted in a custom-made sealed humidity cell. To confirm the reliability and accuracy of the approach, a relatively simple surface-active system was chosen. Specifically, the surface tension of hexanoic acid from 0.1 to 80 mM was measured and compared with the surface tension measurements from the bulk force tensiometer. In addition, SML was collected from a sealed wave-simulation channel facility containing filtered seawater from the southern coast of California in 2019. The surface tension of the SML measured with the AFM showed a statistically significant reduction relative to the bulk tensiometer value. We hypothesize that the difference is due to the AFM's superior sensitivity in detecting the ordering of the surfactant multilayers on the interface.

EXPERIMENTAL SECTION

Bulk Solutions of Hexanoic Acid and Sea Surface Microlayer Samples. Hexanoic acid was purchased from Sigma-Aldrich and used without additional purification. It was dissolved in an ultrapure water (18 MΩ·cm) to generate aqueous bulk solutions with molar concentrations ranging from 0.1 to 80 mM. A sea surface microlayer (SML) sample was collected from a wave-simulation channel facility which contained filtered seawater collected from the southern coast of California during the summer of 2019. The filtered seawater was obtained by first passing the collected seawater through an aluminum screen to remove large marine detritus (e.g., seaweed) and then through a precleaned Nitex nylon 50 μm mesh to remove larger particulates and zooplankton. A phytoplankton bloom in the wave-simulation channel was induced by adding nutrients following similar experimental approaches as in the previous wave-flume studies.[15,53] A glass plate sampling method was utilized to collect the SML samples over the course of the bloom lifetime as reported previously.[25,54] Briefly, a glass plate (30 cm × 40 cm) was lowered by hand at a rate of 5 to 6 cm/s into the wave-simulation channel containing the filtered seawater until approximately 30 cm of the plate was submerged, and then it was withdrawn at approximately the same rate. After being withdrawn, the glass plate was suspended in air for approximately 20 s to allow excess seawater to drain off, and then the glass plate was scraped with a Teflon scraper to collect the remainder of adsorbed liquid.[54−56] Previous studies have shown that this approach is expected to yield an SML sample thickness of approximately 50 μm.[16,25,55−57] The collected SML sample was stored under freezing temperature conditions. The same SML stock sample was utilized to perform both the tensiometer and AFM surface tension measurements.

Bulk Surface Tension Measurements. Bulk surface tension measurements were performed on the aqueous hexanoic acid solutions and SML samples (ca. 6 mL) using a Kibron AquaPi force tensiometer (Kibron, Finland) with the Du Noüy-Padday method (macroneedle diameter of approximately 0.5 mm).[45,49] The measurements have been previously described in detail and only briefly summarized here.[45,49] The tensiometer was calibrated using ultrapure water before and after each experiment, and the dyne probe was cleaned with ethanol and water and torched with a flame between measurements.[45,49] The surface tension of bulk solutions was measured as a function of increasing hexanoic acid solute concentrations. The surface tension of the SML sample was measured without further dilutions. At least three repeated measurements were

https://dx.doi.org/10.1021/acs.langmuir.0c03507
Langmuir 2021, 37, 2457−2465

performed for each liquid sample, with the bulk surface tension value reported as a mean value with one standard deviation.

AFM Surface Tension Measurements on the Droplets. Molecular force probe 3D AFM (Asylum Research, Santa Barbara, CA) was used in contact mode for all force spectroscopy measurements at ambient temperature (25 °C) and pressure.[45,49] A custom-made sealed humidity cell was used to provide a sealed environment to minimize the evaporation of the liquid droplet.[45,49] All AFM experiments were performed at ∼50% relative humidity. High aspect ratio, constant-diameter Ag_2Ga nanoneedles (NN-HAR-FM60, Nauga Needles) with a nominal spring constant of 2.7−3.3 N/m and a radius of 25−100 nm were used for surface tension measurements.[36,45,49] The radius of the nanoneedle was calibrated by performing force measurements on a reference ultrapure water droplet with known surface tension (72.0 mN/m at 25 °C).[58] The resultant value was also compared with a scanning electron microscopy image of each nanoneedle. The nanoneedle radius calibration was repeated both before and after each measurement to ensure no significant change in the probe radius. If the calibrated radius of the nanoneedle differed by more than 10% before and after each AFM experiment, then the data were discarded and the experiment was repeated with a new nanoneedle.[45,49]

A droplet containing aqueous hexanoic acid solution at various concentrations and a droplet of SML were placed on a silicon wafer substrate inside the sealed humidity cell.[45] Each droplet had a typical diameter of 5−7 mm and a height of 2 to 3 mm. Force measurements were collected over the approximate center of the droplet with a 1 Hz scan rate. Upon indenting the nanoneedle several hundred nanometers into the air−liquid interface, the nanoneedle movement was paused within the droplet for 1 to 2 s of dwell time. The nanoneedle was then retracted away from the droplet with a constant pulling rate of 2 μm/s. For each force plot, the maximum retention force was measured and used to quantify the surface tension of the droplet using a previously reported method.[45,49] At least five consecutive force plots were collected for each sample. AFM surface tension data is reported as the mean value, and error bars correspond to one standard deviation.

RESULTS AND DISCUSSION

Calibration of the AFM Nanoneedle Radius. A constant-radius Ag_2Ga nanoneedle was used to probe the liquid droplet surface tension using the AFM. For each nanoneedle used, a calibration step was performed to accurately determine the nanoneedle radius, $R_{nanoneedle}$. First, scanning electron microscopy (SEM) micrographs of the nanoneedle were obtained (Figure 1A, SEM-estimated nanoneedle radius of 120 ± 30 nm for this particular AFM probe).[45] The reported uncertainty of the radius is due to the limited spatial resolution of the SEM.[49] Second, to more accurately calibrate the nanoneedle radius, contact mode AFM force spectroscopy was performed on an ultrapure water droplet which has a known surface tension value at a given temperature (72.0 mN/m at 25 °C).[58] Figure 1B shows the representative force profile where the interaction forces between the nanoneedle and the ultrapure water droplet surface were measured as a function of the tip−sample separation, otherwise known as the distance between the nanoneedle apex and droplet surface.[45] The y axis shows the measured force divided by the circumference of the nanoneedle apex. Positions A−F correspond to the changing nanoneedle vertical position relative to the droplet surface. Upon approach from position A approximately 2 μm away from the droplet surface, the nanoneedle is pulled into the droplet surface by the meniscus formed between the nanoneedle and the surface (position A to B). Then, the nanoneedle indents the droplet, followed by dwelling (or no dwelling) inside the droplet (position C). The dwell refers to maintaining a constant, fixed nanoneedle position within the droplet for a specific time (1 to 2 s in this study). The nanoneedle then retracts away from the droplet (position D). This maximum retention force (F_{ret}) corresponds to the force between the nanoneedle and the droplet meniscus when the contact angle approaches zero (position E).[45] Further retraction of the nanoneedle away from the droplet surface results in rupturing of the meniscus, and the nanoneedle returns to its original position (position F). The maximum retention force can be related to the surface tension of the droplet using eq 1,[45,49]

$$F_{ret} = 2\pi R_{nanoneedle}\sigma \quad (1)$$

where σ is the surface tension of the liquid droplet at a given solute concentration, relative humidity, and temperature. In the aforementioned example, the radius of the nanoneedle is measured to be $R_{nanoneedle}$ = 120 ± 1 nm, which is in excellent agreement with the benchmark radius value of 120 ± 30 nm obtained using the SEM. The measured radius of the nanoneedle was then utilized to quantify the surface tension of liquid droplet samples.

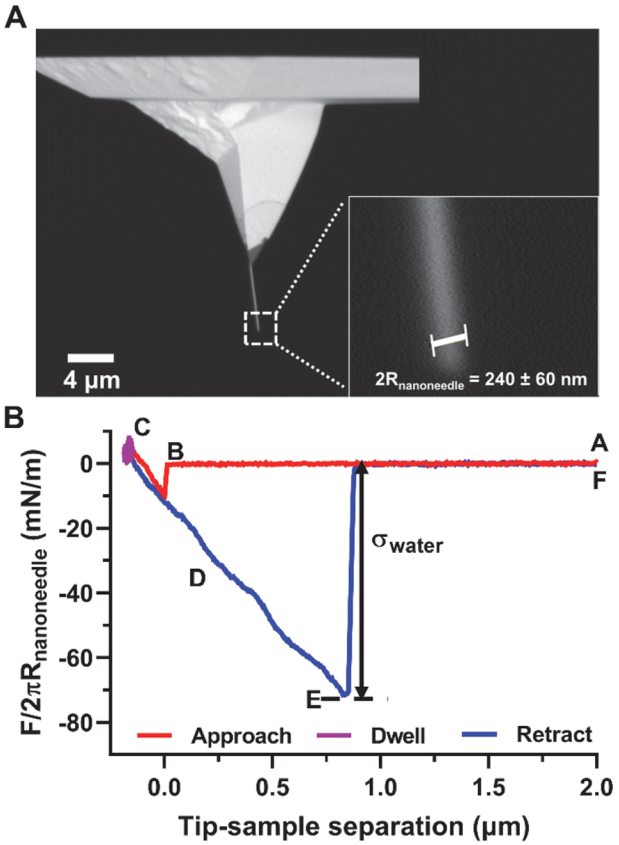

Figure 1. (A) SEM image of a constant-diameter Ag_2Ga nanoneedle with the SEM-determined tip radius of $R_{nanoneedle}$ = 120 ± 30 nm. (B) Representative force divided by the corresponding tip circumference versus the tip−sample separation profile collected over an approximate center on an ultrapure water droplet. The red line corresponds to the nanoneedle approaching the droplet surface, the purple line is the dwell in contact within the droplet, and the blue line is the nanoneedle retracting away from the droplet surface. Symbols A−F correspond to the changing nanoneedle vertical position relative to the droplet surface.

https://dx.doi.org/10.1021/acs.langmuir.0c03507
Langmuir 2021, 37, 2457−2465

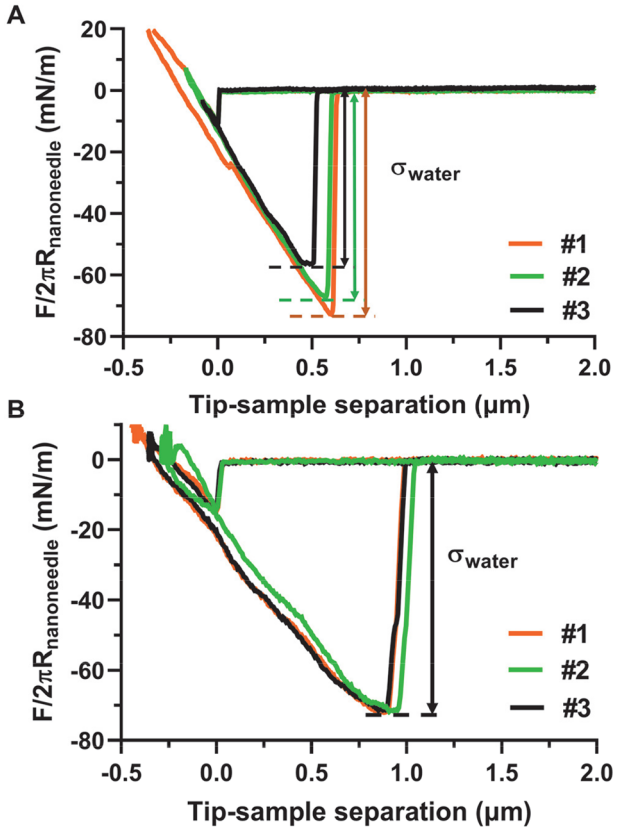

Figure 2. (A) Representative consecutive force divided by the corresponding tip circumference versus tip−sample separation distance profiles (1−3) collected on an ultrapure water droplet without a dwell time. (B) Representative consecutive force versus tip−sample separation distance profiles (1−3) collected on an ultrapure water droplet with a 1 s dwell time.

To ensure that the repeated consecutive force measurements are reproducible, we experimentally determined the ideal dwell time in this study (Figure 2). Note that the dwell time should be varied depending on the liquid sample's volume, viscosity, and composition. In the absence of the dwell time, the maximum retention force measured over an ultrapure water droplet for the initial measurement (force plot 1) exhibited a decreasing trend in the measured force with each consecutive measurement (Figure 2A). This indicates that the dwell time may be necessary in order to measure accurate and consistent retention forces for the liquid droplet. On the other hand, utilizing a 1 s dwell time resulted in closer overlap and more consistent maximum retention force measurements over repeated measurements (Figure 2B). This is likely due to the time required for the interfacial molecules, meniscus, and probe to reach the full equilibrium state. Subsequent surface tension data were obtained using the same dwell time.

Surface Tension Measurements on the Bulk Solutions and Droplets. All AFM measurements were conducted at ambient temperature (25 °C) in a sealed humidity cell (~50% relative humidity) containing a hexanoic acid droplet placed on a silicon wafer substrate. Figure 3A−F shows illustrative force profiles collected at an approximate center on the droplets with selected concentrations. Since the force plots were collected using different nanoneedles with varying diameters, each force measurement was normalized by the corresponding nanoneedle circumference ($2\pi R_{nanoneedle}$) where the radius of the nanoneedle was calibrated using ultrapure water as described in the previous section. In all cases, the indentation distance of the nanoneedle into the droplet surface ranged from 0.3 to 1.2 μm. With increasing concentration, the data show decreasing maximum retention forces and the increasing frequency of multiple but small rupturing events during the retraction. The increasing frequency of multiple rupturing events is likely indicative of the meniscus breaking events at multiple pinning points across the nanoneedle surface (e.g., defects on the surface) as it retracts away from the droplet surface, as reported previously.[36] In general, surface-active molecules such as hexanoic acid preferentially partition to the air−water interface and form (sub)mono- and multilayers, decreasing the surface tension of the droplet.[59−61] Therefore, the increasing frequency of multiple pinning events as the hexanoic acid concentration increases may be indicative of the formation of mono/multilayers at the droplet surface−nanoneedle interface.

On the basis of the measurements of the retention force for hexanoic acid droplets at various concentrations and by using eq 1, the AFM-based surface tension values were determined for each concentration. The surface tension was also measured using the force tensiometer. Figure 4 shows the comparison between the AFM and bulk tensiometer surface tension measurements as a function of the hexanoic acid concentration. Over the entire concentration range (0.1−80 mM), both methods report similar surface tension values despite significantly different indentation depths. Specifically, the typical indentation depth for the bulk tensiometer method is 1−10 mm, whereas that for the AFM it is within the range of 0.3−1.2 μm.[44,62] Despite these differences, however, the two data sets of surface tension measurements overlap well. This was expected because hexanoic acid is a relatively simple one-component model system compared to the nascent SSA or other systems (e.g., SML) that are composed of mixtures of different organic and inorganic species with varying surface activities. While hexanoic acid molecules can form mono/multilayer surface films at the air−liquid interface, the thickness of the film is expected to be significantly less than the AFM probing distance used here (i.e., 0.3 μm or greater). Thus, the measured surface tension values from both methods are expected to be similar and represent the bulk response. The close overlap between two data sets confirms the accuracy of the AFM-based surface tension measurements. Additionally, because of a significantly smaller probing depth compared to the bulk tensiometer method, the AFM-based surface tension method is likely applicable to other aqueous liquid−air interfaces with nano and microscale thicknesses and/or when a limited amount of sample is available (e.g., ca. 200 μL for the AFM and several milliliters for the bulk tensiometer).

To further test the applicability of the AFM surface tension method on more complex systems that include multiple surface-active and surface-inactive components, the approach was extended to study the surface tension of the SML from the wave-simulation channel, which was collected during the peak of a phytoplankton bloom in seawater. During the peak bloom, a significant number of various surfactants can be expected to accumulate at the SML interface and form surface films, including a complex mixture of proteins, lipids, glycopeptides−lipid−oligosaccharide complexes, and pigments.[2,3] Previous studies have measured the concentration for some of these chemical compounds in SML and reported the average and one standard deviation concentration values for the total

https://dx.doi.org/10.1021/acs.langmuir.0c03507
Langmuir 2021, 37, 2457−2465

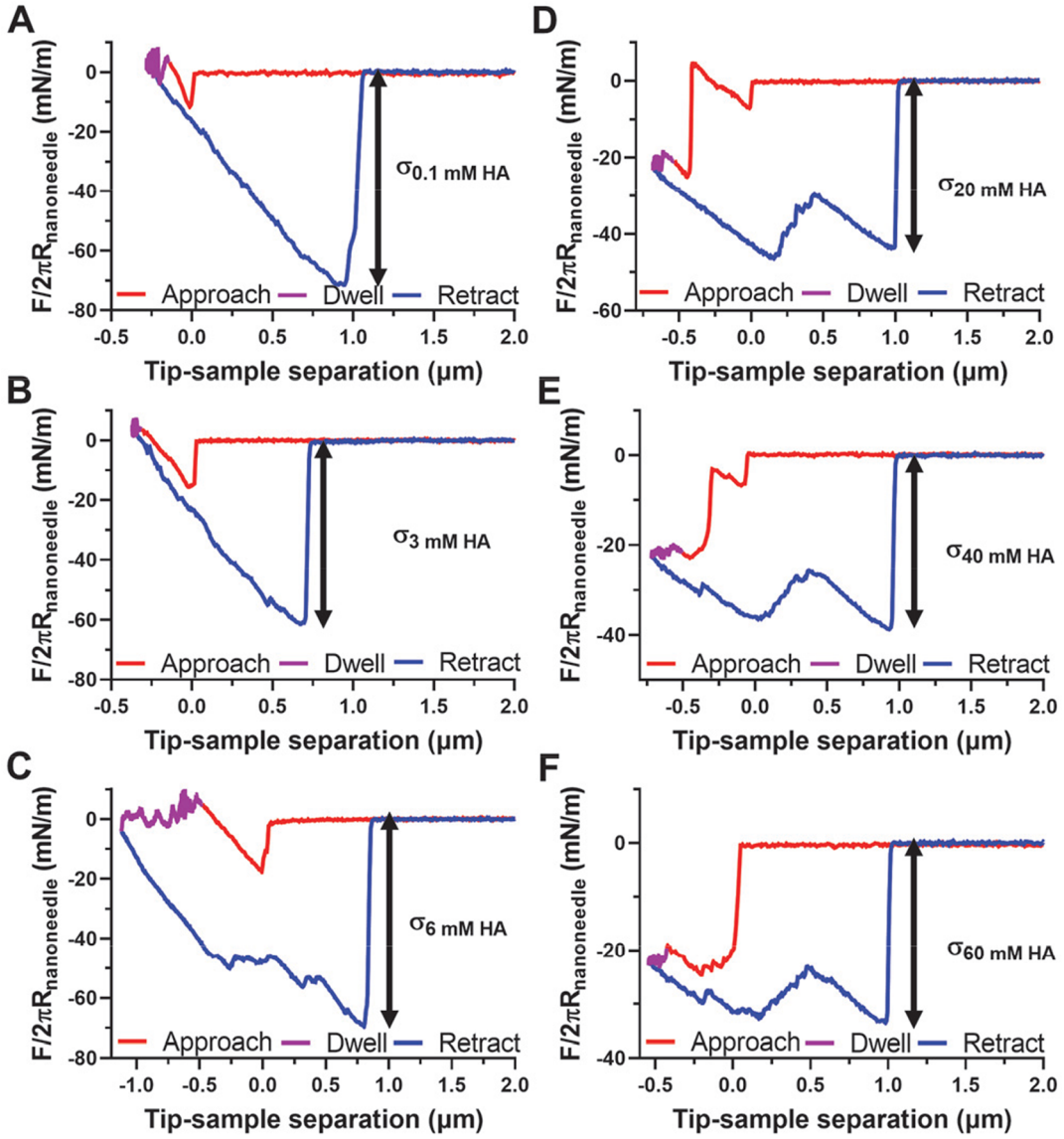

Figure 3. Representative force divided by the corresponding tip circumference versus tip−sample separation profiles (A−F) collected over the approximate center of a hexanoic acid droplet with increasing concentration from 0.1 to 60 mM. Red, purple, and blue lines correspond to the approach, dwell, and retraction from the droplet surface, respectively.

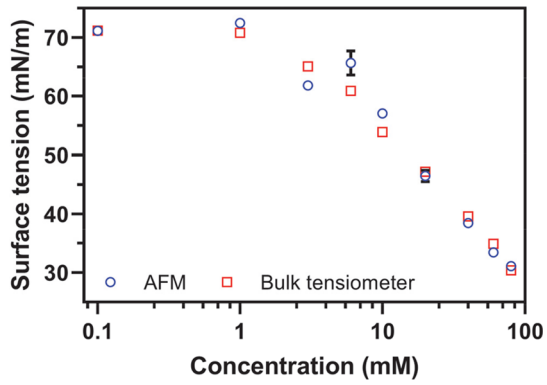

Figure 4. Surface tension data of the hexanoic acid aqueous solution as a function of molar concentration. Blue dots and red squares correspond to the surface tension measurements using the AFM and bulk tensiometer, respectively. In most cases, the error bars (one standard deviation) are smaller than the symbol size.

organic carbon, dissolved combined carbohydrates, total hydrolyzable amino acids, and free amino acids as 127 ± 33 μM, 1111 ± 550 nM, 770 ± 359 nM, and 151 ± 104 nM, respectively.[4,14] Thus, the SML presents an excellent opportunity to test the AFM surface tension method on a highly complex multicomponent sample where a gradient in concentration and the complex formation of the mono- and multilayer surface film structure should be present on a nanometer-to-micrometer length scale.[6,25,26]

Figure 5 shows the representative force profile collected on the SML droplet. All force profiles showed a single rupture event without multiple pinning events, unlike that for the hexanoic acid droplets at higher concentration. Generally, the SML is a highly complex system with a heterogeneous mixture of surfactants with relatively lower concentrations (in the range of μM),[2] significantly lower than several mM concentrations for hexanoic acid droplets where multiple rupture events were observed as shown in Figure 3. On the basis of the measured retention force and using eq 1, the AFM surface tension of the

https://dx.doi.org/10.1021/acs.langmuir.0c03507
Langmuir 2021, 37, 2457−2465

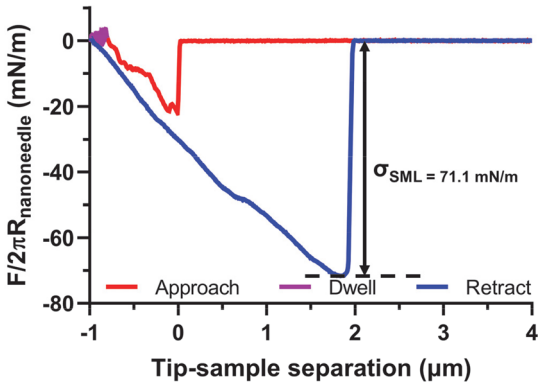

Figure 5. Representative force divided by the corresponding tip circumference versus the tip−sample separation profile collected on a SML droplet from a wave- simulation channel study.

SML was determined to be 71.1 ± 0.3 mN/m, whereas the bulk tensiometer analysis resulted in 73.6 ± 0.1 mN/m. The AFM surface tension for the SML is thus 2.5 mN/m lower than the bulk tensiometer value. An unpaired t test ($P < 0.0001$) confirmed a statistically significant difference between the two measured surface tension values. It is noteworthy that the AFM surface tension for the SML is also 0.9 mN/m lower than that for ultrapure water (72.0 mN/m), indicating the suppression of the surface tension consistent with the expected presence of surfactants at the interface. We tentatively attribute the difference between the AFM and bulk tensiometer surface tension values to the structural and chemical complexity of SML, differences in the probing depth for each method, and the time scale required for the surface film to restructure during the needle retracting away from the liquid. Compared to the binary hexanoic acid−water model system, the SML is a mixture of surface-active and surface-inactive chemical species that can form surface films with a complex multilayers structure at the SML−air interface.[2,4,19,27] Because the probing distances between the two methods differ by several orders of magnitude, the AFM surface tension is likely more reflective of the localized concentration of surfactants within 1 μm or less from the air−liquid interface (the length scale is also comparable to the bubble film at a bursting thickness of 10−1000 nm), while the tensiometer result represents more of the overall bulk volume sample response, which accounts for not only the surfactants at the very top of the interface but also the surface-inactive compounds from the lower layers.[22,23] Given that the very top SML interface largely governs the selective transfer of various species from the SML to sea spray aerosols, the AFM-measured localized surface tension is expected to be a more representative value to consider in order to accurately describe and model such transfer.[5,14,19]

Additionally, the difference in the needle pulling rate and surface film restructuring time scale needed to reach equilibrium could play a role in the observed SML surface tension variation between the AFM and bulk tensiometer measurements. A typical time scale for forming a closely packed surface film for the hexanoic acid−air interface is on the order of milliseconds, while that for a more complex multicomponent system such as SML−air is expected to be significantly longer (e.g., seconds to minutes).[60,63−66] The restructuring time scales of the hexanoic acid and SML surface films were determined in previous studies using the Langmuir trough surface pressure plots and the stress relaxation measurements.[63,65,66] The film restructuring time for the hexanoic acid molecules was reported to be on the order of 5 ms, while that for the SML surface films was between 5 and 25 s and in some cases as long as 30 min.[63,65,66] In the current study, the pulling rate of the AFM nanoneedle is 2 μm/s and the pulling rate of the macroneedle in the bulk tensiometer is ∼0.4 mm/s. Thus, the timescales required to pull each needle by 1 μm as an example would be 500 and 2.5 ms for the AFM and force tensiometer, respectively. Therefore, if the surface film restructuring timescale is comparable to or longer than the timescale of the surface tension measurement, then the film will not be able to reach the equilibrium state during needle retraction. In this regard, the close overlap of the surface tension values between the AFM and bulk tensiometer approach on the hexanoic acid−water samples can be further rationalized by the relatively short time (i.e., milliseconds) required for the hexanoic acid to reform the surface film, indicating that both measurements are reflective of the liquid in the equilibrium state.[60,63] For the SML, however, the time required to form an equilibrated surface film is much longer (i.e., seconds), and thus the force tensiometer surface tension measurement likely corresponds more closely to the non-equilibrium surface film.[24,65,66] In the case of AFM, a 1 to 2 s dwell time coupled with the limited (sub)microscopic indentation depths and nanosized needle diameter likely corresponds to the surface tension measurements of the SML surface film−air interface that is expected to be closer to the equilibrium state. Therefore, the AFM approach is expected to be highly relevant to quantifying the surface tension within a microscale liquid−air interface of liquid samples with a complex probing-distance-dependent sublayer structure of surface films, such as SML with comparatively low concentrations of various surfactants.

■ CONCLUSIONS

The AFM-based force measurements method with a constant-diameter nanoneedle tip was utilized to directly quantify the surface tension of aqueous liquid−air interfaces with (sub)-micrometer indentation distances at ambient temperature and pressure. The samples studied in this work consisted of surface-active hexanoic acid aqueous solutions at various concentrations and the SML sample collected from a wave-simulation channel study during the peak in the phytoplankton bloom in seawater. Ultrapure water was used as a calibration sample to quantify the radius of the AFM nanoneedle. Measured surface tension values on the hexanoic acid droplets using the AFM method were in excellent agreement with the bulk tensiometer data over the entire concentration range from 0.1 to 80 mM, thus validating the AFM method. The surface tension results on the SML sample showed statistically significant differences between the two methods. The difference was tentatively attributed to (sub)microscopic indentation distances for the AFM method where the SML sample can be expected to display an indentation-dependent surface film with sublayers of surface-active species at variable concentrations, while the tensiometer data represent the bulk volume sample response. Our work is expected to enable a more accurate and quantitative understanding of the surface tension of a microscale thin liquid−air interface, particularly those that contain a varying distribution of surface-active compounds as a function of distance from the air−liquid interface.

https://dx.doi.org/10.1021/acs.langmuir.0c03507
Langmuir 2021, 37, 2457−2465

AUTHOR INFORMATION

Corresponding Author

Alexei V. Tivanski − *Department of Chemistry, University of Iowa, Iowa City, Iowa 52242, United States;* orcid.org/0000-0002-1528-2421; Email: alexei-tivanski@uiowa.edu

Authors

Chathuri P. Kaluarachchi − *Department of Chemistry, University of Iowa, Iowa City, Iowa 52242, United States;* orcid.org/0000-0003-2538-3952

Hansol D. Lee − *Department of Chemistry, University of Iowa, Iowa City, Iowa 52242, United States;* orcid.org/0000-0002-2091-776X

Yiling Lan − *Department of Chemistry, University of Iowa, Iowa City, Iowa 52242, United States;* orcid.org/0000-0001-9273-106X

Thiranjeewa I. Lansakara − *Department of Chemistry, University of Iowa, Iowa City, Iowa 52242, United States;* orcid.org/0000-0002-9995-882X

Complete contact information is available at: https://pubs.acs.org/10.1021/acs.langmuir.0c03507

Author Contributions

Surface tension experiments and data analysis were performed by C.P.K. and Y.L. The interpretation of the results and manuscript writing were performed through the contributions of all authors. All authors have given approval to the final version of the manuscript.

Notes

The authors declare no competing financial interest.

ACKNOWLEDGMENTS

This work was funded by the National Science Foundation through the Center for Aerosol Impacts on Chemistry of the Environment under grant no. CHE 1305427. Any opinions, findings, and conclusions or recommendations expressed in this material are those of the authors and do not necessarily reflect the views of the National Science Foundation. The data for this publication can be retrieved from the U.C. San Diego Library Digital Collections (https://doi.org/10.6075/J0ZW1JGC).

REFERENCES

(1) Prather, K. A.; Bertram, T. H.; Grassian, V. H.; Deane, G. B.; Stokes, M. D.; DeMott, P. J.; Aluwihare, L. I.; Palenik, B. P.; Azam, F.; Seinfeld, J. H.; Moffet, R. C.; Molina, M. J.; Cappa, C. D.; Geiger, F. M.; Roberts, G. C.; Russell, L. M.; Ault, A. P.; Baltrusaitis, J.; Collins, D. B.; Corrigan, C. E.; Cuadra-Rodriguez, L. A.; Ebben, C. J.; Forestieri, S. D.; Guasco, T. L.; Hersey, S. P.; Kim, M. J.; Lambert, W. F.; Modini, R. L.; Mui, W.; Pedler, B. E.; Ruppel, M. J.; Ryder, O. S.; Schoepp, N. G.; Sullivan, R. C.; Zhao, D. F. Bringing the ocean into the laboratory to probe the chemical complexity of sea spray aerosol. *Proc. Natl. Acad. Sci. U. S. A.* **2013**, *110* (19), 7550−7555.

(2) Roslan, R. N.; Hanif, N. M.; Othman, M. R.; Azmi, W. N. F. W.; Yan, X. X.; Ali, M. M.; Mohamed, C. A. R.; Latif, M. T. Surfactants in the sea-surface microlayer and their contribution to atmospheric aerosols around coastal areas of the Malaysian peninsula. *Mar. Pollut. Bull.* **2010**, *60* (9), 1584−1590.

(3) Engel, A.; Sperling, M.; Sun, C. C.; Grosse, J.; Friedrichs, G. Organic Matter in the Surface Microlayer: Insights From a Wind Wave Channel Experiment. *Front. Mar. Sci.* **2018**, *5*, 5.

(4) Engel, A.; Galgani, L. The organic sea-surface microlayer in the upwelling region off the coast of Peru and potential implications for air-sea exchange processes. *Biogeosciences* **2016**, *13* (4), 989−1007.

(5) Cochran, R. E.; Jayarathne, T.; Stone, E. A.; Grassian, V. H. Selectivity Across the Interface: A Test of Surface Activity in the Composition of Organic-Enriched Aerosols from Bubble Bursting. *J. Phys. Chem. Lett.* **2016**, *7* (9), 1692−1696.

(6) Wang, X. F.; Deane, G. B.; Moore, K. A.; Ryder, O. S.; Stokes, M. D.; Beall, C. M.; Collins, D. B.; Santander, M. V.; Burrows, S. M.; Sultana, C. M.; Prather, K. A. The role of jet and film drops in controlling the mixing state of submicron sea spray aerosol particles. *Proc. Natl. Acad. Sci. U. S. A.* **2017**, *114* (27), 6978−6983.

(7) Quinn, P. K.; Collins, D. B.; Grassian, V. H.; Prather, K. A.; Bates, T. S. Chemistry and Related Properties of Freshly Emitted Sea Spray Aerosol. *Chem. Rev.* **2015**, *115* (10), 4383−4399.

(8) Cochran, R. E.; Laskina, O.; Jayarathne, T.; Laskin, A.; Laskin, J.; Lin, P.; Sultana, C.; Lee, C.; Moore, K. A.; Cappa, C. D.; Bertram, T. H.; Prather, K. A.; Grassian, V. H.; Stone, E. A. Analysis of Organic Anionic Surfactants in Fine and Coarse Fractions of Freshly Emitted Sea Spray Aerosol. *Environ. Sci. Technol.* **2016**, *50* (5), 2477−2486.

(9) Lee, H. D.; Morris, H. S.; Laskina, O.; Sultana, C. M.; Lee, C.; Jayarathne, T.; Cox, J. L.; Wang, X. F.; Hasenecz, E. S.; DeMott, P. J.; Bertram, T. H.; Cappa, C. D.; Stone, E. A.; Prather, K. A.; Grassian, V. H.; Tivanski, A. V. Organic Enrichment, Physical Phase State, and Surface Tension Depression of Nascent Core-Shell Sea Spray Aerosols during Two Phytoplankton Blooms. *Acs Earth Space Chem.* **2020**, *4* (4), 650−660.

(10) Hasenecz, E. S.; Kaluarachchi, C. P.; Lee, H. D.; Tivanski, A. V.; Stone, E. A. Saccharide Transfer to Sea Spray Aerosol Enhanced by Surface Activity, Calcium, and Protein Interactions. *Acs Earth Space Chem.* **2019**, *3* (11), 2539−2548.

(11) Petras, D.; Minich, J. J.; Cancelada, L. B.; Torres, R. R.; Kunselman, E.; Wang, M.; White, M. E.; Allen, E. E.; Prather, K. A.; Aluwihare, L. I.; Dorrestein, P. C. Non-targeted tandem mass spectrometry enables the visualization of organic matter chemotype shifts in coastal seawater. *Chemosphere* **2021**, *271*, 129450.

(12) Ault, A. P.; Moffet, R. C.; Baltrusaitis, J.; Collins, D. B.; Ruppel, M. J.; Cuadra-Rodriguez, L. A.; Zhao, D. F.; Guasco, T. L.; Ebben, C. J.; Geiger, F. M.; Bertram, T. H.; Prather, K. A.; Grassian, V. H. Size-Dependent Changes in Sea Spray Aerosol Composition and Properties with Different Seawater Conditions. *Environ. Sci. Technol.* **2013**, *47* (11), 5603−5612.

(13) Cochran, R. E.; Laskina, O.; Trueblood, J. V.; Estillore, A. D.; Morris, H. S.; Jayarathne, T.; Sultana, C. M.; Lee, C.; Lin, P.; Laskin, J.; Laskin, A.; Dowling, J. A.; Qin, Z.; Cappa, C. D.; Bertram, T. H.; Tivanski, A. V.; Stone, E. A.; Prather, K. A.; Grassian, V. H. Molecular Diversity of Sea Spray Aerosol Particles: Impact of Ocean Biology on Particle Composition and Hygroscopicity. *Chem-Us* **2017**, *2* (5), 655−667.

(14) Jayarathne, T.; Sultana, C. M.; Lee, C.; Malfatti, F.; Cox, J. L.; Pendergraft, M. A.; Moore, K. A.; Azam, F.; Tivanski, A. V.; Cappa, C. D.; Bertram, T. H.; Grassian, V. H.; Prather, K. A.; Stone, E. A. Enrichment of Saccharides and Divalent Cations in Sea Spray Aerosol During Two Phytoplankton Blooms. *Environ. Sci. Technol.* **2016**, *50* (21), 11511−11520.

(15) Schill, S. R.; Collins, D. B.; Lee, C.; Morris, H. S.; Novak, G. A.; Prather, K. A.; Quinn, P. K.; Sultana, C. M.; Tivanski, A. V.; Zimmermann, K.; Cappa, C. D.; Bertram, T. H. The Impact of Aerosol Particle Mixing State on the Hygroscopicity of Sea Spray Aerosol. *ACS Cent. Sci.* **2015**, *1* (3), 132−141.

(16) Cunliffe, M.; Engel, A.; Frka, S.; Gašparović, B.; Guitart, C.; Murrell, J. C.; Salter, M.; Stolle, C.; Upstill-Goddard, R.; Wurl, O. Sea surface microlayers: A unified physicochemical and biological perspective of the air-ocean interface. *Prog. Oceanogr.* **2013**, *109*, 104−116.

(17) Wurl, O.; Ekau, W.; Landing, W. M.; Zappa, C. J. Sea surface microlayer in a changing ocean - A perspective. *Elementa-Sci. Anthrop* **2017**, *5*, 31.

(18) Soloviev, A. V.; Lukas, R.; Donelan, M. A.; Haus, B. K.; Ginis, I. The air-sea interface and surface stress under tropical cyclones. *Sci. Rep.* **2015**, *4*, 5306.

(19) Ciuraru, R.; Fine, L.; van Pinxteren, M.; D'Anna, B.; Herrmann, H.; George, C. Photosensitized production of functionalized and unsaturated organic compounds at the air-sea interface. *Sci. Rep.* **2015**, *5*, 12741.
(20) Engel, A.; Bange, H. W.; Cunliffe, M.; Burrows, S. M.; Friedrichs, G.; Galgani, L.; Herrmann, H.; Hertkorn, N.; Johnson, M.; Liss, P. S.; Quinn, P. K.; Schartau, M.; Soloviev, A.; Stolle, C.; Upstill-Goddard, R. C.; van Pinxteren, M.; Zäncker, B. The Ocean's Vital Skin: Toward an Integrated Understanding of the Sea Surface Microlayer. *Frontiers in Marine Science* **2017**, *4* (165), DOI: 10.3389/fmars.2017.00165.
(21) Lass, K.; Friedrichs, G. Revealing structural properties of the marine nanolayer from vibrational sum frequency generation spectra. *J. Geophys. Res.* **2011**, DOI: 10.1029/2010JC006609.
(22) Burrows, S. M.; Ogunro, O.; Frossard, A. A.; Russell, L. M.; Rasch, P. J.; Elliott, S. M. A physically based framework for modeling the organic fractionation of sea spray aerosol from bubble film Langmuir equilibria. *Atmos. Chem. Phys.* **2014**, *14* (24), 13601–13629.
(23) Modini, R. L.; Russell, L. M.; Deane, G. B.; Stokes, M. D. Effect of soluble surfactant on bubble persistence and bubble-produced aerosol particles. *J. Geophys Res-Atmos* **2013**, *118* (3), 1388–1400.
(24) Boniewicz-Szmyt, K.; Pogorzelski, S. J. Evolution of natural sea surface films: a new quantification formalism based on multidimensional space vector. *Environ. Sci. Pollut. Res.* **2018**, *25* (5), 4826–4836.
(25) Zhang, Z. B.; Liu, L. S.; Liu, C. Y.; Cai, W. J. Studies on the sea surface microlayer - II. The layer of sudden change of physical and chemical properties. *J. Colloid Interface Sci.* **2003**, *264* (1), 148–159.
(26) Zhengbin, Z.; Liansheng, L.; Zhijian, W.; Jun, L.; Haibing, D. Physicochemical Studies of the Sea Surface Microlayer: I. Thickness of the Sea Surface Microlayer and Its Experimental Determination. *J. Colloid Interface Sci.* **1998**, *204* (2), 294–299.
(27) Schmidt, R.; Schneider, B. The effect of surface films on the air-sea gas exchange in the Baltic Sea. *Mar. Chem.* **2011**, *126* (1), 56–62.
(28) Hunter, K. A.; Liss, P. S. Input of Organic Material to Oceans - Air-Sea Interactions and Organic Chemical Composition of Sea-Surface. *Mar. Chem.* **1977**, *5* (4–6), 361–379.
(29) Frew, N. M.; Nelson, R. K. Scaling of Marine Microlayer Film Surface Pressure-Area Isotherms Using Chemical Attributes. *J. Geophys. Res.* **1992**, *97* (C4), 5291–5300.
(30) Cunliffe, M.; Upstill-Goddard, R. C.; Murrell, J. C. Microbiology of aquatic surface microlayers. *FEMS Microbiology Reviews* **2011**, *35* (2), 233–246.
(31) Ciuraru, R.; Fine, L.; van Pinxteren, M.; D'Anna, B.; Herrmann, H.; George, C. Unravelling New Processes at Interfaces: Photochemical Isoprene Production at the Sea Surface. *Environ. Sci. Technol.* **2015**, *49* (22), 13199–13205.
(32) Donaldson, D. J.; George, C. Sea-Surface Chemistry and Its Impact on the Marine Boundary Layer. *Environ. Sci. Technol.* **2012**, *46* (19), 10385–10389.
(33) Steinhart, M. Physics and Chemistry of Interfaces. By Hans-Jürgen Butt, Karlheinz Graf, and Michael Kappl. *Angew. Chem., Int. Ed.* **2004**, *43* (27), 3510a–3511.
(34) Harkins, W. D.; Jordan, H. F. A method for the determination of surface and interfacial tension from the maximum pull on a ring. *J. Am. Chem. Soc.* **1930**, *52*, 1751–1772.
(35) Freud, B. B.; Freud, H. Z. A theory of the ring method for the determination of surface tension. *J. Am. Chem. Soc.* **1930**, *52*, 1772–1782.
(36) Yazdanpanah, M. M.; Hosseini, M.; Pabba, S.; Berry, S. M.; Dobrokhotov, V. V.; Safir, A.; Keynton, R. S.; Cohn, R. W. Micro-Wilhelmy and Related Liquid Property Measurements Using Constant-Diameter Nanoneedle-Tipped Atomic Force Microscope Probes. *Langmuir* **2008**, *24* (23), 13753–13764.
(37) Hasegawa, T.; Karasawa, M.; Narumi, T., Modeling and measurement of the dynamic surface tension of surfactant solutions. *J. Fluids Eng.* **2008**, *130* (8), DOI: 10.1115/1.2956597.
(38) Bzdek, B. R.; Power, R. M.; Simpson, S. H.; Reid, J. P.; Royall, C. P. Precise, contactless measurements of the surface tension of picolitre aerosol droplets. *Chemical Science* **2016**, *7* (1), 274–285.
(39) Metcalf, A. R.; Boyer, H. C.; Dutcher, C. S. Interfacial Tensions of Aged Organic Aerosol Particle Mimics Using a Biphasic Microfluidic Platform. *Environ. Sci. Technol.* **2016**, *50* (3), 1251–1259.
(40) Berry, J. D.; Neeson, M. J.; Dagastine, R. R.; Chan, D. Y. C.; Tabor, R. F. Measurement of surface and interfacial tension using pendant drop tensiometry. *J. Colloid Interface Sci.* **2015**, *454*, 226–237.
(41) Juza, J. The pendant drop method of surface tension measurement: Equation interpolating the shape factor tables for several selected planes. *Czech. J. Phys.* **1997**, *47* (3), 351–357.
(42) Padday, J. F.; Pitt, A. R.; Pashley, R. M. Menisci at a Free Liquid Surface - Surface-Tension from Maximum Pull on a Rod. *J. Chem. Soc., Faraday Trans. 1* **1975**, *71*, 1919–1931.
(43) Tariq, M.; Freire, M. G.; Saramago, B.; Coutinho, J. A. P.; Lopes, J. N. C.; Rebelo, L. P. N. Surface tension of ionic liquids and ionic liquid solutions. *Chem. Soc. Rev.* **2012**, *41* (2), 829–868.
(44) Fataraite, E.; Jankauskaite, V.; Marazas, G.; Milasiene, D.; Zukiene, K. Viscosity and Surface Properties of Melamine-Formaldehyde Resin Composition. *Mater. Sci-Medzg* **2009**, *15* (3), 250–254.
(45) Lee, H. D.; Estillore, A. D.; Morris, H. S.; Ray, K. K.; Alejandro, A.; Grassian, V. H.; Tivanski, A. V. Direct Surface Tension Measurements of Individual Sub-Micrometer Particles Using Atomic Force Microscopy. *J. Phys. Chem. A* **2017**, *121* (43), 8296–8305.
(46) Dupréde Baubigny, J.; Benzaquen, M.; Fabié, L.; Delmas, M.; Aimé, J.-P.; Legros, M.; Ondarçuhu, T. Shape and Effective Spring Constant of Liquid Interfaces Probed at the Nanometer Scale: Finite Size Effects. *Langmuir* **2015**, *31* (36), 9790–9798.
(47) Uddin, M. H.; Tan, S. Y.; Dagastine, R. R. Novel Characterization of Microdrops and Microbubbles in Emulsions and Foams Using Atomic Force Microscopy. *Langmuir* **2011**, *27* (6), 2536–2544.
(48) Tang, Y.; Cheng, S. The meniscus on the outside of a circular cylinder: From microscopic to macroscopic scales. *J. Colloid Interface Sci.* **2019**, *533*, 401–408.
(49) Morris, H. S.; Grassian, V. H.; Tivanski, A. V. Humidity-dependent surface tension measurements of individual inorganic and organic submicrometre liquid particles (vol 6, pg 3242, 2015). *Chem. Sci.* **2015**, *6* (10), 6021–6021.
(50) Hritz, A. D.; Raymond, T. M.; Dutcher, D. D. A method for the direct measurement of surface tension of collected atmospherically relevant aerosol particles using atomic force microscopy. *Atmos. Chem. Phys.* **2016**, *16* (15), 9761–9769.
(51) Rodenbucher, C.; Wippermann, K.; Korte, C. Atomic Force Spectroscopy on Ionic Liquids. *Appl. Sci.* **2019**, *9* (11), 2207.
(52) Shimizu, K.; Tariq, M.; Freitas, A. A.; Padua, A. A. H.; Lopes, J. N. C. Self-Organization in Ionic Liquids: From Bulk to Interfaces and Films. *J. Braz. Chem. Soc.* **2015**, DOI: 10.5935/0103-5053.20150274.
(53) Lee, H. D.; Wigley, S.; Lee, C.; Or, V. W.; Hasenecz, E. S.; Stone, E. A.; Grassian, V. H.; Prather, K. A.; Tivanski, A. V. Physicochemical Mixing State of Sea Spray Aerosols: Morphologies Exhibit Size Dependence. *Acs Earth Space Chem.* **2020**, *4* (9), 1604–1611.
(54) Anderson, Z. T.; Cundy, A. B.; Croudace, I. W.; Warwick, P. E.; Celis-Hernandez, O.; Stead, J. L. A rapid method for assessing the accumulation of microplastics in the sea surface microlayer (SML) of estuarine systems. *Sci. Rep.* **2018**, *8*, 9428.
(55) Wurl, O.; Zimmer, L.; Cutter, G. A. Arsenic and phosphorus biogeochemistry in the ocean: Arsenic species as proxies for P-limitation. *Limnol. Oceanogr.* **2013**, *58* (2), 729–740.
(56) Carlson, D. J. Surface Microlayer Phenolic Enrichments Indicate Sea-Surface Slicks. *Nature* **1982**, *296* (5856), 426–429.
(57) Shinki, M.; Wendeberg, M.; Vagle, S.; Cullen, J. T.; Hore, D. K. Characterization of adsorbed microlayer thickness on an oceanic glass plate sampler. *Limnol. Oceanogr.: Methods* **2012**, *10*, 728–735.

(58) Nikitas, P.; Pappalouisi, A. Thermodynamic and Modelistic Study of Surface Solutions - Aqueous-Solutions Containing 2-Butanol. *J. Phys. Chem.* **1990**, *94* (1), 361−370.
(59) Ruehl, C. R.; Wilson, K. R. Surface Organic Mono layers Control the Hygroscopic Growth of Submicrometer Particles at High Relative Humidity. *J. Phys. Chem. A* **2014**, *118* (22), 3952−3966.
(60) Soule, M. C. K.; Blower, P. G.; Richmond, G. L. Effects of atmospherically important solvated ions on organic acid adsorption at the surface of aqueous solutions. *J. Phys. Chem. B* **2007**, *111* (49), 13703−13713.
(61) Pierson, F. W.; Whitaker, S. Studies of the drop-weight method for surfactant solutions. II. Experimental results for water and surfactant solutions. *J. Colloid Interface Sci.* **1976**, *54*, 219−230.
(62) Wålinder, M.; Johansson, I. Measurement of Wood Wettability by the Wilhelmy Method. Part 1. Contamination of Probe Liquids by Extractives. *Holzforschung* **2001**, *55*, 21−32.
(63) Fainerman, V. B.; Zholob, S. A.; Miller, R.; Joos, P. Non-diffusional adsorption dynamics of surfactants at the air/water interface: adsorption barrier or non-equilibrium surface layer. *Colloids Surf., A* **1998**, *143* (2−3), 243−249.
(64) Hansen, R. S.; Wallace, T. C. The Kinetics of Adsorption of Organic Acids at the Water-Air Interface. *J. Phys. Chem.* **1959**, *63* (7), 1085−1091.
(65) Pogorzelski, S. J.; Stortini, A. M.; Loglio, G. Natural Surface-Film Studies in Shallow Coastal Waters of the Baltic and Mediterranean Seas. *Cont. Shelf Res.* **1994**, *14* (13−14), 1621.
(66) Pogorzelski, S. J.; Kogut, A. D. Structural and thermodynamic signatures of marine microlayer surfactant films. *J. Sea Res.* **2003**, *49* (4), 347−356.

https://dx.doi.org/10.1021/acs.langmuir.0c03507
Langmuir 2021, 37, 2457−2465